Flowerlike Spreading of Micellar Films during Emulsion Drop Evaporation

Teng Dong,* Kristo Kotsi, Teke Xu, Takeshi Kobayashi, Alexander Moriarty, and Panagiota Angeli†
ThAMeS Multiphase, Department of Chemical Engineering, University College London, London WC1E 7JE, United Kingdom

Ian McRobbie
Innospec Ltd., Oil Sites Road, Ellesmere Port, Cheshire CH65 4EY, United Kingdom

Alberto Striolo
School of Sustainable Chemical, Biological and Materials Engineering, The University of Oklahoma, Norman, Oklahoma 73019, USA

(Received 7 February 2024; accepted 26 August 2024; published 23 October 2024)

We investigated the film spreading during the evaporation of submillimeter oil-in-water emulsion droplets on a solid surface, and observed a novel phenomenon where the film follows a two-layer spreading. In combination with the instability at the film front, the spreading front acquires a flowerlike pattern. The emergence of the two-layer structure is attributed to micelles within the oil film that yield an oscillating disjoining pressure. By considering both the slipping condition and the disjoining pressure, a scaling analysis is carried out that agrees well with the observed film spreading dynamics. The film spreading follows Tanner's law initially, while it becomes faster at a later stage, where the film radius follows $r \sim t^{1/2}$ for weak slip and $r \sim t^{3/8}$ for strong slip conditions.

DOI: 10.1103/PhysRevLett.133.174001

Evaporation of sessile drops has been extensively studied. Prominent discoveries include the shrinkage regimes and diffusive models that describe the contact angle dependence of the evaporation rate [1–5]. Also well-known is the 'coffee ring' phenomenon, which is associated with the convective flow within the drops [6,7]. Drop spreading and evaporation is ubiquitous among processes such as inkjet printing [8], spray cooling [9], and agrochemical applications [10,11] where drops often consist of complex formulations. Recently, there has been an increasing interest in the evaporation of colloidal drops with solid particles dispersed in them [5,12–16]. In contrast, the understanding of the emulsion drops evaporation remains limited. The few available studies mainly report spatial distributions and size evolution of the dispersed droplets during the evaporation of emulsion drops or films [17–20]. A recent study reported that the accumulated droplets tend to coalesce, forming a continuous film that spreads out; however, no in-depth analysis was carried out on the spreading dynamics [21].

*Contact author: teng.dong.15@ucl.ac.uk
†Contact author: p.angeli@ucl.ac.uk

In this Letter, we report intriguing phenomena observed during the evaporation of oil-in-water emulsion drops. We found that the oil droplets brought into the vicinity of the contact line by convection coalesce to yield a continuous film that spreads beyond the initial contact area. The film spreads maintaining two well-defined layers, forming flowerlike patterns. After an initial stage, the spreading rates of both layers are found to be much faster than Tanner's law predicted [22].

The emulsion is prepared by mixing the 5 cSt silicone oil (10% w/w) that contains Span 80 (2% w/w), an oil-soluble surfactant, within continuous deionized water (88% w/w). The mixture was homogenized in a Pulse 150® instrument for 5 min, resulting in most dispersed drop sizes lower than 1 μm, as shown in Fig. 1(a). VWR® microscope glass slides that yield a contact angle of 30° for water drops were selected as the solid surface. The glass slides were immersed in ethanol and deionized water for 20 min each, and then dried by compressed nitrogen. Drops of submillimeter sizes were deposited on the glass surface using a needle (id = 0.15 mm). The evaporation was observed with a Zeiss® microscope with the observation area covered by a lid whose size is much larger than the drop to prevent disturbances from the surroundings [Fig. 1(b)]. The local temperature is set 25 °C and the humidity is around 33% for all the evaporation tests.

After deposition, the drops take a few milliseconds to open from a round shape to a sessile state on the solid

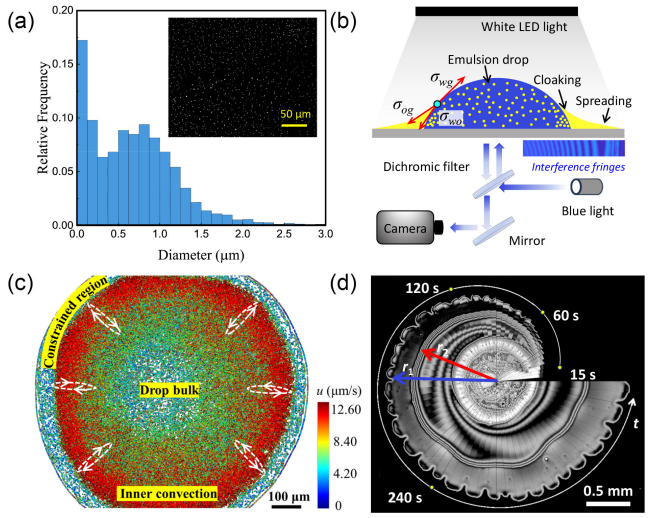

FIG. 1. (a) Size distribution of the dispersed droplets in 10% silicone oil emulsion. (b) Experimental setup for drop evaporation. σ_{wg}, σ_{og}, and σ_{wo} indicate the tension along water-gas, oil-gas and water-oil interfaces. (c) Convection current in the drop with white arrows indicating the direction. (d) Reconstruction of the consecutive images of the spreading film.

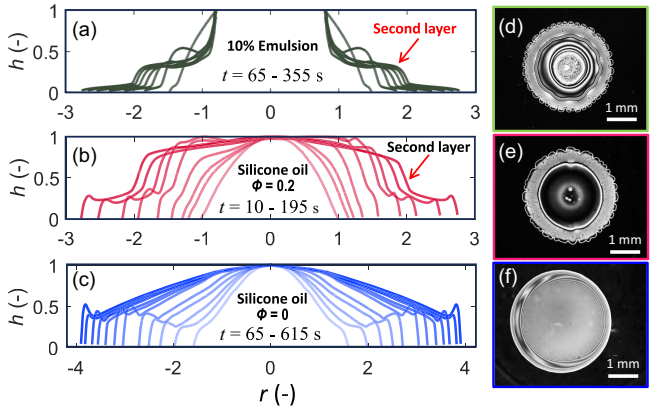

FIG. 2. Film evolution for drops of (a) 10% emulsion, (b) silicone oil at $\phi = 0.2$, and (c) pure silicone oil at $\phi = 0$. The radius r is normalized with the initial radius of the drop and the height h is normalized with the maximum height at each time instant. Representative interference images at a later stage of the spreading corresponding cases (a), (b), and (c) are shown in (d), (e), and (f).

surface; as we do not focus on this stage, we start the recording at around 1 s afterwards. As shown in Fig. 1(c) and Movie 1, strong convection currents appear in the bulk of the drop due to uneven evaporation rate along the drop surface, the Marangoni effect along the water-oil interface, and natural convection [7,12,23]. The Marangoni effect is weak as the convective velocity is of the order of μm/s (see Supplemental Material (SM) [24] for more details). Driven by the convection currents, the dispersed droplets are transported from the drop bulk toward the constrained region where no strong convection is seen. The dispersed droplets in the constrained region coalesce at the periphery to form a thin film of oil that spreads outwards (see Movie 2 in SM [24]). The film thickness was measured with light interference, using blue light with wavelength $\lambda = 475$ nm, as illustrated in Fig. 1(b). Driven by the surface tension difference $\sim(\sigma_{wg} - \sigma_{og} - \sigma_{wo})$ at the water-oil-air contact line, the drop is partially cloaked with the thin oil film [39–42] (Movie 2 [24]). As cloaking eventually occurs far from the front line, the outward spreading is not influenced significantly by the cloaking phenomenon.

The film counterintuitively spreads as two layers, with a sharp difference in thickness between the two as shown in Figs. 1(d) and 2(a) (Movie 3 [24]). To the best of our knowledge, this phenomenon has not been reported previously. A two-layer pattern also appears in the spreading of Span 80-laden silicon oil drops at $\phi = 0.2$, which is much larger than the critical micelle concentration (CMC), as shown in Fig. 2(b) and Movie 4 [24]. In contrast, the two layers are not observed during the spreading of pure silicone oil drops or silicone oil drops with Span 80 at $\phi = 2 \times 10^{-4}$, a concentration lower than the CMC; in these cases, a smooth transition exists from the bulk to the film front and only small bulges are present due to the perturbations in the transverse direction [43–45] [see Fig. 2(c) and Movie 5 [24]]. Even if the bottom layer is regarded as a precursor film, there should not be a sharp increase in the thickness [46–48]. Because of this, the two-layer spreading is not attributed to the coalescence of the dispersed oil droplets that supply the fluid in the film. It is worth noting that the silicone oils with Span 80 at the two concentrations below and above CMC are Newtonian fluids [24]. Fingering patterns are seen at the edge of the spreading film for all cases due to the contact line instability, which helps the flowerlike spreading. Here, we do not focus on the fingers in particular as the instability does not grow under our experimental conditions (see SM [24] for more details).

As the thickness of the film layer reduces to ~100 nm or less for all the cases shown in Fig. 2, the disjoining pressure becomes important and drives the film spread. The disjoining pressure arises from long-range Van der Waals, short-range steric, and electrostatic forces [49]. The combined effect induces an oscillating pressure, which gives rise to the formation of layering [50,51]. Notably, for simple liquids, this layering diminishes as the oscillations are gradually damped when the film thickness increases to approximately 10 times the molecular size and above [49,52,53]. For colloidal and micellar systems, however, experimental measurements show distinct oscillatory forces are still pronounced at film thicknesses exceeding 50 nm [54–61]. Our atomic force microscopy measurements indicate that the micelles generated in the silicone oil at $\phi = 0.2$, which are expected to be of ~30 nm in diameter, sustain the oscillations of the disjoining pressure in thicker films (see SM [24] for more details).

Hereafter, we analyze the spreading dynamics of the thin film, where lubrication theory applies as the film thickness h is much smaller than the spreading radius r. Span 80 was found to only decrease the water-oil interfacial tension but it did not affect the oil-air surface tension. Thus, Marangoni effects are not expected to affect the oil spreading. A fourth-order nonlinear equation can be used to describe the film spreading [25,62–64],

$$\frac{\partial h}{\partial t} = -\frac{1}{3\mu}\nabla\cdot[\sigma h^3\nabla\nabla^2 h - \rho g h^3\nabla h] + \nabla\cdot[D(h)\nabla h]. \quad (1)$$

The first term on the right side of Eq. (1) corresponds to the capillary force and the gravity force, while the second term is related to the disjoining pressure Π, where $D(h)$ is the diffusion coefficient given by [25,62]

$$D(h) = -\frac{h^3}{3\mu}\frac{d\Pi}{dh}. \quad (2)$$

The first term on the right of Eq. (1) has self-similar solution $h(r,t) = t^{-2\alpha}H(rt^{-\alpha})$ considering constant volume of spreading film $V = \int 2\pi r h(r,t)dr$. If the capillary force dominates, the radius follows $r \sim t^{1/10}$ as Tanner's law predicts [22,25,62], while for gravity-driven spreading, the film radius follows $r \sim t^{1/8}$ [65–67]. Gravity can be neglected as the size of the droplet is way smaller than the capillary length $l_c = \sqrt{\sigma_{\text{oil}}/\rho_{\text{oil}}g}$. Tanner's law has been found to successfully predict many experimental findings not only with simple liquids but also polymers and liquid crystals [25,68,69]. Our results show that for micellar films, Tanner's law is only followed in the initial spreading stage of both the bottom and the second layer of the film for all fluids studied. We attribute this to the disjoining pressure that is not considered in Tanner's theory [22].

To check whether the disjoining pressure is involved in spreading, we track the evolution of the contact angle θ at the film edge. Previous researchers, as summarized by Tanner [22], attributed the advancing of the contact line to the balance between the surface tension and the viscous forces $\sigma_{lg}(1-\cos\theta) \sim \mu UR/h$, where U is the film spreading velocity and R is the length over which the film is straight and $h = R\tan\theta$ is valid, as shown in Fig. 3(a). For small contact angles, we obtain $\theta \sim Ca^{1/3}$ [22,69], where $Ca = \mu U/\sigma_{lg}$ is the capillary number. Other researchers rescaled the viscous term to be $\sim\mu UR/\lambda$ by considering a strong Navier slip condition [70,71], where λ is the slip length as shown in Fig. 3(b). The relation then becomes $\theta \sim Ca^{1/2}(R/\lambda)^{1/2}$.

We extracted θ at the front of the spreading film by measuring the spatial distance at a height difference corresponding to the first couple of fringes in the interference pattern. As shown in Fig. 3(d), for all three cases,

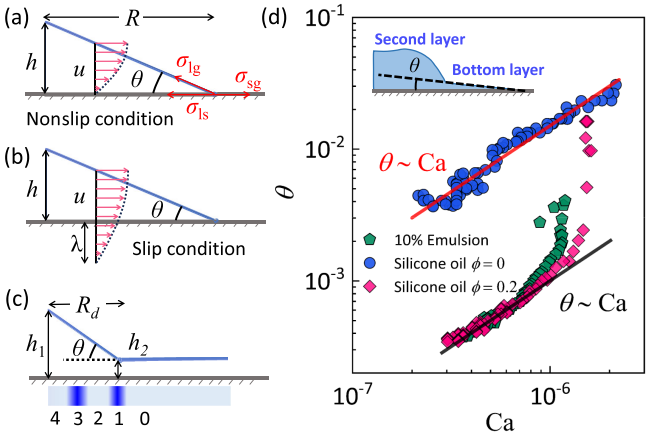

FIG. 3. Schematics of the contact line moving models considering (a) nonslip condition, (b) slip condition, and (c) disjoining pressure. (d) Evolution of the contact angle θ against the capillary number Ca for the bottom layer; the inset illustrates how the contact angle θ is measured.

the contact angle follows $\theta \sim Ca$, which is larger than $\theta \sim Ca^{1/2}$ and larger than Tanner's law $\theta \sim Ca^{1/3}$. It is worth noting that for the emulsion drop and the silicone oil drop with surfactant at $\phi = 0.2$, there are deviations from $\theta \sim Ca$ at the initial stage corresponding to a large value of θ as the bottom layer has not been established yet. This provides evidence that the disjoining pressure Π contributes to the observed phenomena, as discussed below. The disjoining pressure is defined as $\Pi = A/6\pi h^3$ when only the long-range Van der Waals force is considered, where A is the Hamaker constant [44,49,72]. However, in the current experiments, the spreading of the film is analogous to the spreading of nematic liquid crystals, building on the observations by Poulard and Cazabat [73]. This is perhaps due to the assembly of the micelles in the oil film. The similarity does not only include the layering of the spreading film but also the contact angle relation and the spreading law, which will be discussed later. Following Poulard and Cazabat [73], we defined the disjoining pressure as $\Pi = 0.5K\delta^2/h^2$, where K is the bend-splay elastic constant and δ is the angle related to the assembly of the crystals.

If we consider $0.5K\delta^2$ constant and introduce a length scale $a = K\delta^2/2\sigma$, the disjoining pressure becomes $\Pi = a\sigma/h^2$. Balancing the disjoining pressure and the viscous resistance at the film edge and considering a strong slip condition, we obtain $\sigma a(h_1^{-1} - h_2^{-1}) \sim \mu UR_d/\lambda$, where R_d is the distance between positions at the thickness of h_1 and h_2, as shown in Fig. 3(c). For weak slip conditions, we define an average film thickness $h_a = (h_1 + h_2)/2$, and the balance between the capillary and the viscous term becomes $\sigma a(h_1^{-1} - h_2^{-1}) \sim \mu UR_d/h_a$. Considering $\theta \sim (h_1 - h_2)/R_d$, the contact angle relation $\theta \sim Cah_1h_2a/\lambda$ for strong slip and $\theta \sim Cah_1h_2a/h_a$ for weak slip. Both relations lead to $\theta \sim Ca$, given that the heights

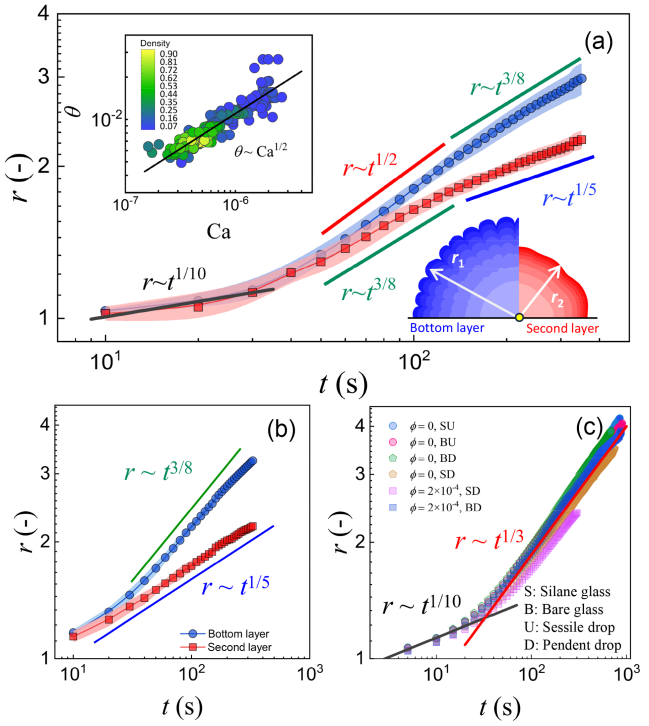

FIG. 4. Film radius evolution during the spreading of (a) 10% emulsion drop, (b) silicone oil drop at $\phi = 0.2$, and (c) silicone oil drop at $\phi <$ CMC. The inset in (a) indicates the change of θ against Ca at the edge of the second layer. In (c), saline surfaces increase the contact angle of water to approximately 90° compared to bare surfaces.

are independent of θ in the current experiments. It is worth noting that, for simple liquids without micelles where $\Pi = A/6\pi h^3$, the relation $\theta \sim Ca$ is again valid when the disjoining pressure is important, as shown by the blue circles for the pure silicone oil drop in Fig. 3(d).

As illustrated in Fig. 4(a), the film radius r only follows Tanner's law ($r \sim t^{1/10}$) in the short beginning of the spreading for both the bottom and the second layer. A new spreading law $r \sim t^{1/2}$ then appears for the bottom layer. Note that for $\Pi = 0.5K\delta^2/h^2$, the coefficient $D(h)$ becomes constant, making Eq. (1) a purely diffusive equation when the disjoining pressure dominates [62]. Accordingly, the film radius follows $r \sim t^{1/2}$. If this is the reason, the scaling law of $r \sim t^{1/2}$ should persist till the end; however, at a later stage, the spreading of the bottom layer deviates, as shown in Fig. 4(a). Thus, we need to analyze the spreading laws $r \sim t^n$ in general, where n is the exponent shown in Fig. 4. For convenience, Eq. (1) is reorganized using the continuous equation $\partial h/\partial t = -Uh'$,

$$h''' = -\frac{3Ca}{h^2 + 3\lambda h} + \frac{2ah'}{h^3}, \tag{3}$$

where $' = \partial/\partial r$ is the space derivative. In Eq. (3) gravity is neglected and the Navier slip condition is taken into account. The film thickness h and the spreading radius r are normalized as $H = h/3\lambda$ and $\xi = r/R$. The dimensionless term H indicates the slipping extent and R represents a length where the film remains straight from the contact point. Accordingly, Eq. (3) becomes

$$H''' = -\frac{3\alpha}{H^2 + H} + \frac{2\beta H'}{H^3}. \tag{4}$$

The term on the left is the capillary term, and the first term on the right is the viscous term where $\alpha = Ca(R/3\lambda)^3$. The second term indicates the disjoining pressure where $\beta = aR^2/(3\lambda)^3$. The balance between the capillary term $\sim H/\xi^3$ and the disjoining pressure $\sim \beta/H^2\xi$ yields $H \sim (\beta\xi^2)^{1/3}$, or $h^3 \sim ar^2$ in a dimensional form. For strong slip conditions where $H \ll 1$, the viscous term is $\sim \alpha/H$. Balancing it to the capillary term, we have $H^2 \sim \alpha\xi^3$, and the dimensional relation $r \sim (3\lambda\sigma_{lg}/\mu)^{3/8}a^{1/4}t^{3/8}$ is derived considering $h^3 \sim ar^2$. The viscous term becomes $\sim \alpha/H^2$ for weak slip where $H \gg 1$. Balancing it to the capillary term, $H^3 \sim \alpha\xi^3$, and the dimensional form is $r \sim (a\sigma/\mu)^{1/2}t^{1/2}$. This explains well the spreading of the bottom layer in the evaporation of 10% emulsion drop. At the intermediate stage of the bottom film spreading, the film thickness $H \gg 1$ that $r \sim t^{1/2}$, while at a later stage, the spreading shifts to $r \sim t^{3/8}$ when the film thickness reduces to $H \ll 1$. For the drop of silicone oil at $\phi = 0.2$, the film evolves into strong slip directly and the radius follows $r \sim t^{3/8}$ without an intermediate weak slip regime [Fig. 4(b)].

For the second layer of the 10% emulsion drop, the film spreading obeys $r \sim t^{3/8}$ and then shifts to $r \sim t^{1/5}$. The spreading of the second layer follows $r \sim t^{3/8}$ initially while it differs from the dynamics of the bottom layer and remains to be explored. As for the spreading law of $r \sim t^{1/5}$ observed in the final stage for both the 10% emulsion drop and the silicone oil drop at $\phi = 0.2$, we believe that gravity plays a role. When gravity dominates, the self-similar solution of Eq. (1) predicts $r \sim t^{1/5}$ in the context of two-dimensional spreading [51]. In this stage, the film radius $r > l_c$, and the influence of the capillary force compared to gravity is reduced. Additionally, the second layer becomes sufficiently thick, causing disjoining pressure to diminish. This is also seen in the evolution of the contact angle at the front of the second layer, which shows $\theta \sim Ca^{1/2}$ rather than $\theta \sim Ca$ in the inset in Fig. 4(a).

The spreading law changes little when the disjoining pressure takes the form of $\Pi = A/6\pi h^3$, resulting in $r \sim t^{1/3}$ for strong slip and $r \sim t^{2/5}$ for weak slip. This is seen in the spreading of silicone oil at $\phi <$ CMC where no micelles are generated. As shown in Fig. 4(c), the law of $r \sim t^{1/3}$ fits well the fast spreading in such conditions. As shown in SM [24], this law is applicable not only to the spreading of

low-viscosity silicone oils but to other liquids such as those used by Mouat *et al.* [26] and Baumgartner *et al.* [27].

In conclusion, we experimentally investigated the simultaneous spread and evaporation of submillimeter emulsion drops. The coalescence of the dispersed oil produces a continuous phase that spreads out under the emulsion drop. A two-layer spreading mechanism, which is analogous to the blooming of flowers, is observed. A similar behavior is also seen in the spreading of drops of silicone oil with Span 80 at a concentration much higher than the CMC, while only a single layer is seen for silicone oil drops with a surfactant concentration below the CMC. This implies that the two-layer spreading is likely due to the micelles in the oil, which produce oscillating disjoining pressure profiles [49,55,62]. When the disjoining pressure and the slip length are both involved, the spreading follows a new law given by $r \sim t^{1/2}$ for weak slip and $r \sim t^{3/8}$ for strong slip, which is much faster than predicted by Tanner's law [22]. The spreading of the second layer follows $r \sim t^{1/5}$ in the later stage driven by gravity. Our work reports novel phenomena and reveals new spreading mechanisms of micellar liquids that have previously remained unexplored. It offers fundamental insights into the structured forces in thin-layer supramolecular systems. The results acquired are expected to offer new knowledge for processes like inkjet printing [8], spreading of agrochemicals [10], film coating [74], and spray cooling [75].

Acknowledgments—The authors acknowledge financial support from EPSRC (EP/V032909/1), Innospec, and the Asahi Glass Chair of Chemical Engineering at the University of Oklahoma.

[1] H. Y. Erbil, G. McHale, and M. Newton, Drop evaporation on solid surfaces: Constant contact angle mode, Langmuir **18**, 2636 (2002).
[2] K. M. Al Balushi, G. Duursma, P. Valluri, K. Sefiane, and D. Orejon, Binary mixture droplet evaporation on microstructured decorated surfaces and the mixed stick–slip modes, Langmuir **39**, 8323 (2023).
[3] R. Picknett and R. Bexon, The evaporation of sessile or pendant drops in still air, J. Colloid Interface Sci. **61**, 336 (1977).
[4] Y. O. Popov, Evaporative deposition patterns: Spatial dimensions of the deposit, Phys. Rev. E **71**, 036313 (2005).
[5] S. P. Thampi and M. G. Basavaraj, Drying drops of colloidal dispersions, Annu. Rev. Chem. Biomol. Eng. **14**, 53 (2023).
[6] P. J. Yunker, T. Still, M. A. Lohr, and A. Yodh, Suppression of the coffee-ring effect by shape-dependent capillary interactions, Nature (London) **476**, 308 (2011).
[7] C. Diddens, Y. Li, and D. Lohse, Competing marangoni and rayleigh convection in evaporating binary droplets, J. Fluid Mech. **914**, A23 (2021).
[8] R. Deng, L. Yang, and C. D. Bain, Combining inkjet printing with emulsion solvent evaporation to pattern polymeric particles, ACS Appl. Mater. Interfaces **10**, 12317 (2018).
[9] M. Shen, B. Q. Li, Q. Yang, Y. Bai, Y. Wang, S. Zhu, B. Zhao, T. Li, and Y. Hu, A modified phase-field three-dimensional model for droplet impact with solidification, Int. J. Multiphase Flow **116**, 51 (2019).
[10] N. Somala, C. Laosinwattana, and M. Teerarak, Formulation process, physical stability and herbicidal activities of cymbopogon nardus essential oil-based nanoemulsion, Sci. Rep. **12**, 10280 (2022).
[11] W. Yang, W. Jia, M. Ou, W. Zhong, L. Jiang, and X. Wang, Effect of physical properties of an emulsion pesticide on the atomisation process and the spatial distribution of droplet size, Agriculture **12**, 949 (2022).
[12] Y. Li, Evaporating multicomponent droplets, Ph.D. thesis, University of Twente, 2020.
[13] H. Tan, S. Wooh, H.-J. Butt, X. Zhang, and D. Lohse, Porous supraparticle assembly through self-lubricating evaporating colloidal ouzo drops, Nat. Commun. **10**, 478 (2019).
[14] J. Gerber, T. M. Schutzius, and D. Poulikakos, Patterning of colloidal droplet deposits on soft materials, J. Fluid Mech. **907**, A39 (2021).
[15] A. Pelosse, É. Guazzelli, and M. Roché, Probing dissipation in spreading drops with granular suspensions, J. Fluid Mech. **955**, A7 (2023).
[16] Y. Li, C. Diddens, T. Segers, H. Wijshoff, M. Versluis, and D. Lohse, Evaporating droplets on oil-wetted surfaces: Suppression of the coffee-stain effect, Proc. Natl. Acad. Sci. U.S.A. **117**, 16756 (2020).
[17] M. Gopu and D. Mampallil, Distributed evaporation of water-in-oil emulsion drops on solid surfaces, Phys. Fluids **34**, 102110 (2022).
[18] A. Kapilashrami, K. Eskilsson, L. Bergström, and M. Malmsten, Drying of oil-in-water emulsions on hydrophobic and hydrophilic substrates, Colloids Surf. A **233**, 155 (2004).
[19] K. Hasegawa and S. Inasawa, Evaporation kinetics of continuous water and dispersed oil droplets, Soft Matter **16**, 8692 (2020).
[20] S. Das, P. R. Waghmare, M. Fan, N. S. K. Gunda, S. S. Roy, and S. K. Mitra, Dynamics of liquid droplets in an evaporating drop: Liquid droplet "coffee stain" effect, RSC Adv. **2**, 8390 (2012).
[21] M. Bittermann, A. Deblais, S. Lépinay, D. Bonn, and N. Shahidzadeh, Deposits from evaporating emulsion drops, Sci. Rep. **10**, 14863 (2020).
[22] L. Tanner, The spreading of silicone oil drops on horizontal surfaces, J. Phys. D **12**, 1473 (1979).
[23] R. Van Gaalen, C. Diddens, H. Wijshoff, and J. Kuerten, Marangoni circulation in evaporating droplets in the presence of soluble surfactants, J. Colloid Interface Sci. **584**, 622 (2021).
[24] See Supplemental Material, which includes Refs. [7,12,16,22,23,25–38], at http://link.aps.org/supplemental/10.1103/PhysRevLett.133.174001, which presents the methodology of the experiments and discussions on the subprocesses of film spreading; videos on the evaporation of emulsion drops and the film spreading under various conditions are included as well.

[25] L. Kondic, Instabilities in gravity driven flow of thin fluid films, SIAM Rev. **45**, 95 (2003).
[26] A. P. Mouat, C. E. Wood, J. E. Pye, and J. C. Burton, Tuning contact line dynamics and deposition patterns in volatile liquid mixtures, Phys. Rev. Lett. **124**, 064502 (2020).
[27] D. A. Baumgartner, S. Shiri, S. Sinha, S. Karpitschka, and N. J. Cira, Marangoni spreading and contracting three-component droplets on completely wetting surfaces, Proc. Natl. Acad. Sci. U.S.A. **119**, e2120432119 (2022).
[28] P. Neogi, Contact line instability in spontaneous spreading of a drop on a solid surface, J. Fluid Mech. **428**, 171 (2001).
[29] T. Dong, W. H. Weheliye, P. Chausset, and P. Angeli, An experimental study on the drop/interface partial coalescence with surfactants, Phys. Fluids **29** (2017).
[30] E. Hecht, *Optics* (Pearson Education India, Harlow, England, 2012).
[31] S. M. Troian, E. Herbolzheimer, and S. A. Safran, Model for the fingering instability of spreading surfactant drops, Phys. Rev. Lett. **65**, 333 (1990).
[32] A. P. Bowles, Y.-T. Hsia, P. M. Jones, J. W. Schneider, and L. R. White, Quasi-equilibrium afm measurement of disjoining pressure in lubricant nano-films I: Fomblin z03 on silica, Langmuir **22**, 11436 (2006).
[33] C. M. Mate, M. R. Lorenz, and V. Novotny, Atomic force microscopy of polymeric liquid films, J. Chem. Phys. **90**, 7550 (1989).
[34] C. M. Mate and V. Novotny, Molecular conformation and disjoining pressure of polymeric liquid films, J. Chem. Phys. **94**, 8420 (1991).
[35] J. Ally, M. Kappl, and H.-J. Butt, Adhesion of particles with sharp edges to air–liquid interfaces, Langmuir **28**, 11042 (2012).
[36] K. A. Emelyanenko, A. M. Emelyanenko, and L. B. Boinovich, Disjoining pressure analysis of the lubricant nanofilm stability of liquid-infused surface upon lubricant depletion, J. Colloid Interface Sci. **618**, 121 (2022).
[37] M. Cachile, M. Schneemilch, A. Hamraoui, and A. Cazabat, Films driven by surface tension gradients, Adv. Colloid Interface Sci. **96**, 59 (2002).
[38] A. Hamraoui, M. Cachile, C. Poulard, and A. Cazabat, Fingering phenomena during spreading of surfactant solutions, Colloids Surf. A **250**, 215 (2004).
[39] X. Yao, Y. Hu, A. Grinthal, T.-S. Wong, L. Mahadevan, and J. Aizenberg, Adaptive fluid-infused porous films with tunable transparency and wettability, Nat. Mater. **12**, 529 (2013).
[40] A. Keiser, L. Keiser, C. Clanet, and D. Quéré, Drop friction on liquid-infused materials, Soft Matter **13**, 6981 (2017).
[41] S. Hardt and G. McHale, Flow and drop transport along liquid-infused surfaces, Annu. Rev. Fluid Mech. **54**, 83 (2022).
[42] J. D. Smith, R. Dhiman, S. Anand, E. Reza-Garduno, R. E. Cohen, G. H. McKinley, and K. K. Varanasi, Droplet mobility on lubricant-impregnated surfaces, Soft Matter **9**, 1772 (2013).
[43] H. E. Huppert, Flow and instability of a viscous current down a slope, Nature (London) **300**, 427 (1982).
[44] R. V. Craster and O. K. Matar, Dynamics and stability of thin liquid films, Rev. Mod. Phys. **81**, 1131 (2009).
[45] D. E. Kataoka and S. M. Troian, A theoretical study of instabilities at the advancing front of thermally driven coating films, J. Colloid Interface Sci. **192**, 350 (1997).
[46] H. P. Kavehpour, B. Ovryn, and G. H. McKinley, Microscopic and macroscopic structure of the precursor layer in spreading viscous drops, Phys. Rev. Lett. **91**, 196104 (2003).
[47] D. Beaglehole, Profiles of the precursor of spreading drops of siloxane oil on glass, fused silica, and mica, J. Phys. Chem. **93**, 893 (1989).
[48] P.-G. De Gennes, Wetting: Statics and dynamics, Rev. Mod. Phys. **57**, 827 (1985).
[49] H. Yin, D. N. Sibley, U. Thiele, and A. J. Archer *et al.*, Films, layers, and droplets: The effect of near-wall fluid structure on spreading dynamics, Phys. Rev. E **95**, 023104 (2017).
[50] F. Heslot, N. Fraysse, and A. Cazabat, Molecular layering in the spreading of wetting liquid drops, Nature (London) **338**, 640 (1989).
[51] D. Bonn, J. Eggers, J. Indekeu, J. Meunier, and E. Rolley, Wetting and spreading, Rev. Mod. Phys. **81**, 739 (2009).
[52] P. Wu, A. Nikolov, and D. Wasan, Capillary dynamics driven by molecular self-layering, Adv. Colloid Interface Sci. **243**, 114 (2017).
[53] O. K. Matar, R. V. Craster, and K. Sefiane, Dynamic spreading of droplets containing nanoparticles, Phys. Rev. E **76**, 056315 (2007).
[54] P. Richetti and P. Kékicheff, Direct measurement of depletion and structural forces in a micellar system, Phys. Rev. Lett. **68**, 1951 (1992).
[55] N. C. Christov, K. D. Danov, Y. Zeng, P. A. Kralchevsky, and R. von Klitzing, Oscillatory structural forces due to nonionic surfactant micelles: Data by colloidal- probe afm vs theory, Langmuir **26**, 915 (2010).
[56] P. Kekicheff and P. Richetti, Direct measurement of interactions in supermolecular fluids and liquid crystals, Pure Appl. Chem. **64**, 1603 (1992).
[57] D. L. Sober and J. Y. Walz, Measurement of long range depletion energies between a colloidal particle and a flat surface in micellar solutions, Langmuir **11**, 2352 (1995).
[58] J. C. Crocker, J. A. Matteo, A. D. Dinsmore, and A. G. Yodh, Entropic attraction and repulsion in binary colloids probed with a line optical tweezer, Phys. Rev. Lett. **82**, 4352 (1999).
[59] M. Ludwig and R. von Klitzing, Recent progress in measurements of oscillatory forces and liquid properties under confinement, Curr. Opin. Colloid Interface Sci. **47**, 137 (2020).
[60] A. D. Nikolov and D. T. Wasan, The foam film's stepwise thinning phenomenon and role of oscillatory forces, Adv. Colloid Interface Sci. **303**, 102636 (2022).
[61] C. Ochoa, S. Gao, S. Srivastava, and V. Sharma, Foam film stratification studies probe intermicellar interactions, Proc. Natl. Acad. Sci. U.S.A. **118**, e2024805118 (2021).
[62] S. Mechkov, A. Cazabat, and G. Oshanin, Post-tanner spreading of nematic droplets, J. Phys. Condens. Matter **21**, 464134 (2009).
[63] K. E. Pang and L. Ó Náraigh, A mathematical model and mesh-free numerical method for contact-line motion in lubrication theory, Environ. Fluid Mech. **22**, 301 (2022).

[64] J. A. Diez and L. Kondic, Contact line instabilities of thin liquid films, Phys. Rev. Lett. **86**, 632 (2001).
[65] J. Lopez, C. A. Miller, and E. Ruckenstein, Spreading kinetics of liquid drops on solids, J. Colloid Interface Sci. **56**, 460 (1976).
[66] A. M. Cazabat and M. A. C. Cohen, Dynamics of wetting: Effects of surface roughness, J. Phys. Chem. **90**, 5845 (1986).
[67] S. C. Durian, S. Dillavou, K. Markin, A. Portales, B. O. T. Maldonado, W. Irvine, P. E. Arratia, and D. J. Durian, Spatters and spills: Spreading dynamics for partially wetting droplets, Phys. Fluids **34** (2022).
[68] D. Ausserré, A. M. Picard, and L. Léger, Existence and role of the precursor film in the spreading of polymer liquids, Phys. Rev. Lett. **57**, 2671 (1986).
[69] A. Mohammad Karim, A review of physics of moving contact line dynamics models and its applications in interfacial science, J. Appl. Phys. **132** (2022).
[70] H.-H. Wei, H.-K. Tsao, and K.-C. Chu, Slipping moving contact lines: Critical roles of de Gennes's 'foot'in dynamic wetting, J. Fluid Mech. **873**, 110 (2019).
[71] Y.-C. Liao, Y.-C. Li, and H.-H. Wei, Drastic changes in interfacial hydrodynamics due to wall slippage: Slip-intensified film thinning, drop spreading, and capillary instability, Phys. Rev. Lett. **111**, 136001 (2013).
[72] B. Dai, L. G. Leal, and A. Redondo, Disjoining pressure for nonuniform thin films, Phys. Rev. E **78**, 061602 (2008).
[73] C. Poulard and A. Cazabat, Spontaneous spreading of nematic liquid crystals, Langmuir **21**, 6270 (2005).
[74] B. Li, Q.-B. Zhu, C. Cui, C. Liu, Z.-H. Wang, S. Feng, Y. Sun, H.-L. Zhu, X. Su, Y.-M. Zhao *et al.*, Patterning of wafer-scale mxene films for high-performance image sensor arrays, Adv. Mater. **34**, 2201298 (2022).
[75] J. Li and P. B. Weisensee, Low Weber number droplet impact on heated hydrophobic surfaces, Exp. Therm. Fluid. Sci. **130**, 110503 (2022).